# Supporting information

# Bismuth Vacancy Tuned Bismuth Oxybromide Ultrathin Nanosheets towards Photocatalytic $CO_2$ Reduction

Jun Di[1,2‡], Chao Chen[2,‡], Chao Zhu[2,‡], Pin Song[2,‡], Jun Xiong[1], Mengxia Ji[1], Jiadong Zhou[2], Qundong Fu[2], Manzhang Xu[2], Wei Hao[2], Jiexiang Xia[1,*], Shuzhou Li[2], Huaming Li[1], Zheng Liu[2,*]

[1] School of Chemistry and Chemical Engineering, Institute for Energy Research, Jiangsu University, 301 Xuefu Road, Zhenjiang, 212013, P. R. China

[2] Center for Programmable Materials, School of Materials Science & Engineering, Nanyang Technological University, Singapore 639798, Singapore

‡ These authors contributed equally to this work.

*Corresponding author: z.liu@ntu.edu.sg; xjx@ujs.edu.cn

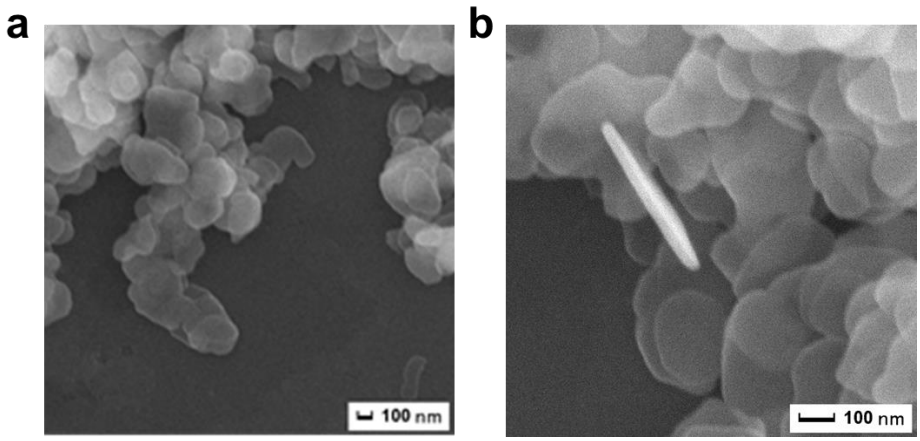


**Figure S1**. (a, b) SEM images of BiOBr nanosheets.

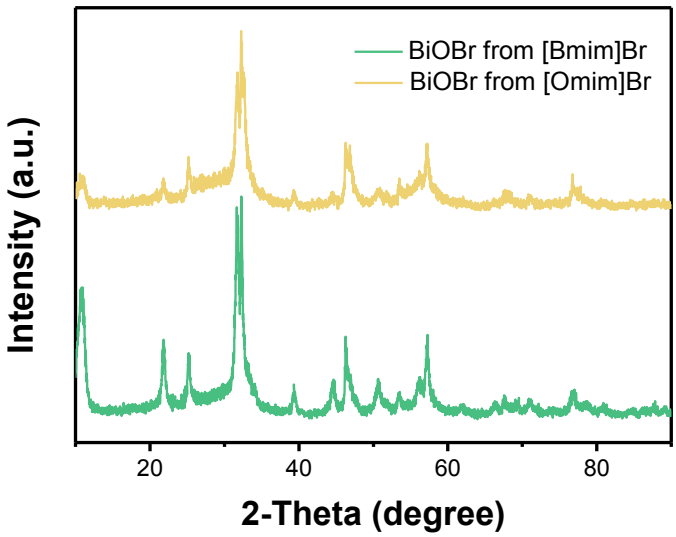


**Figure S2**. XRD pattern of BiOBr materials prepared from [Bmim]Br and [Omim]Br via the procedure to prepare $V_{Bi}$-BiOBr UNs.

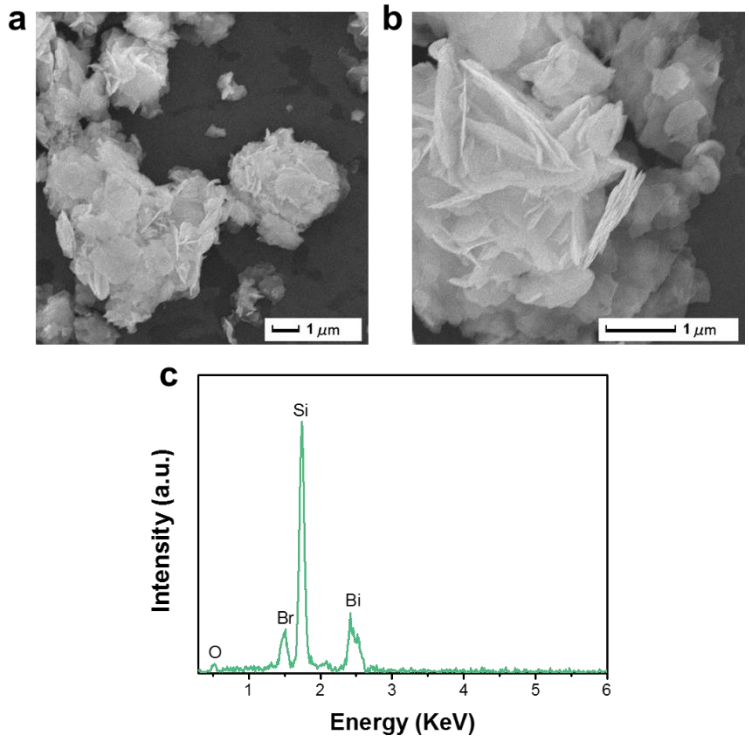


**Figure S3**. (a, b) SEM images and (c) EDS of BiOBr material prepared from [Bmim]Br.

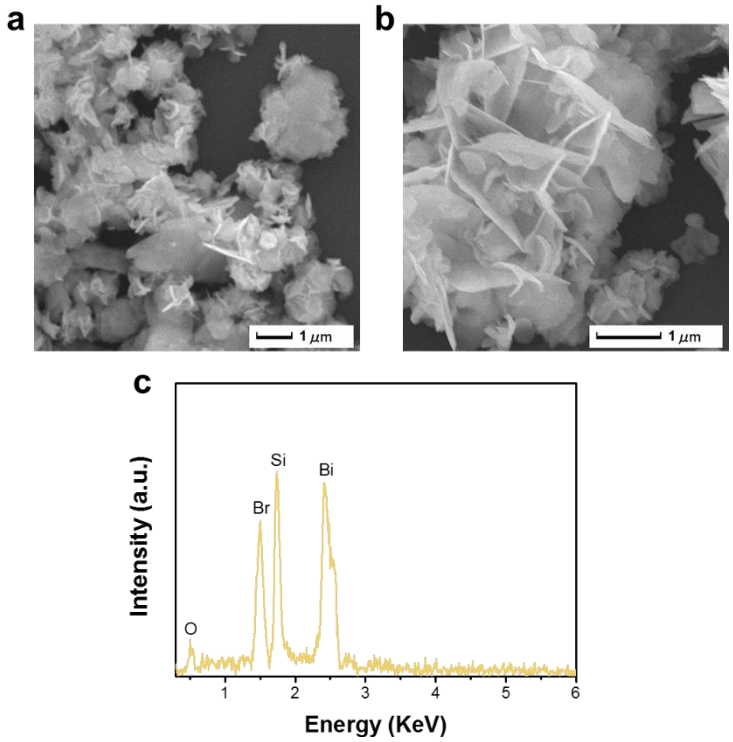


**Figure S4**. (a, b) SEM images and (c) EDS of BiOBr material prepared from [Omim]Br.

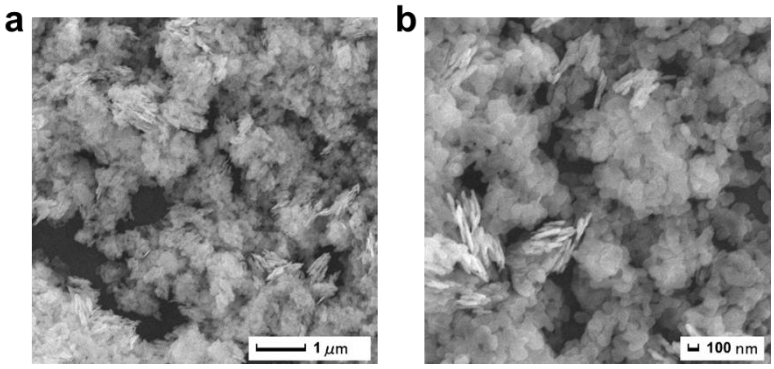


**Figure S5**. (a, b) SEM images of BiOBr material prepared from KBr.

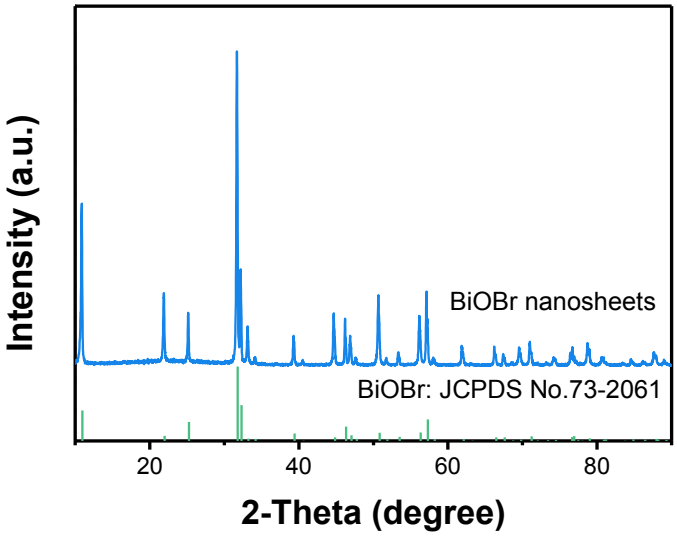


**Figure S6**. XRD pattern of BiOBr nanosheets.

As displayed in **Figure S7a**, Bi, O, Br and C elements are observed in the survey spectrum. The carbon peak was come from the adventitious carbon on the surface of the sample. It can be seen from **Figure S7b** that the two peaks at 159.3 eV and 164.7 eV are assigned to Bi 4f7/2 and Bi 4f5/2, which indicating the $Bi^{3+}$ in the $V_{Bi}$-BiOBr UNs. In the high-resolution Br spectrum (**Figure S7c**), the peak binding energy of 68.4 eV is ascribed to Br 3d, which is characteristic of $Br^-$ in the $V_{Bi}$-BiOBr UNs.

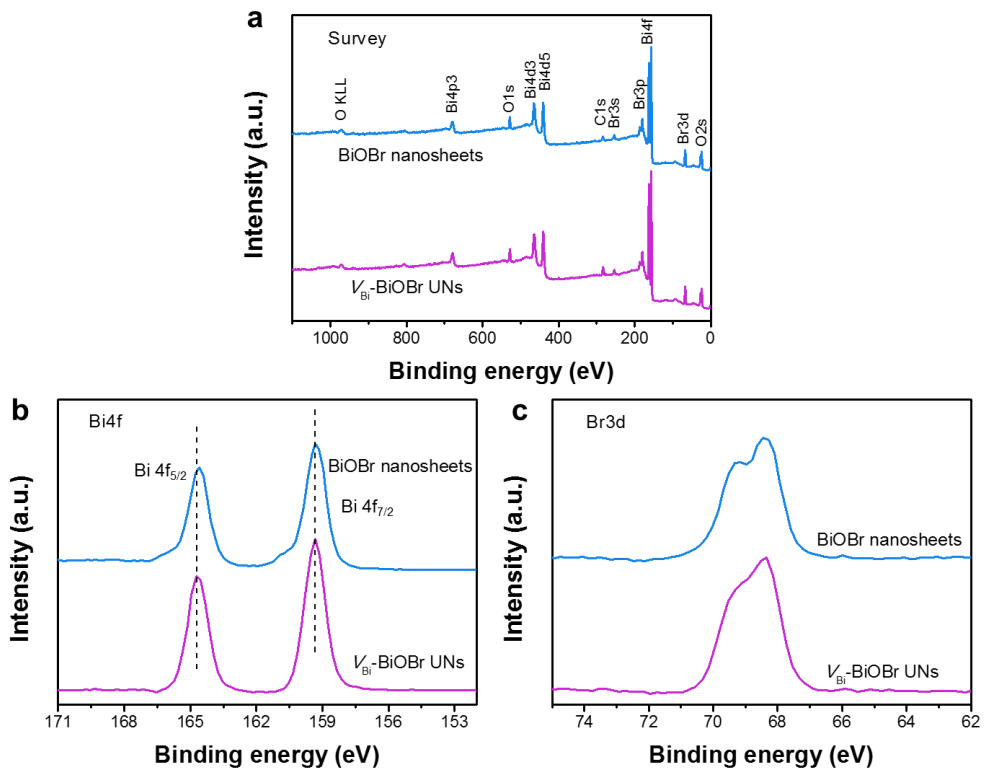


**Figure S7**. XPS spectra of $V_{Bi}$-BiOBr UNs and BiOBr nanosheets. (a) Survey of the sample, (b) Bi 4f, (c) Br 3d.

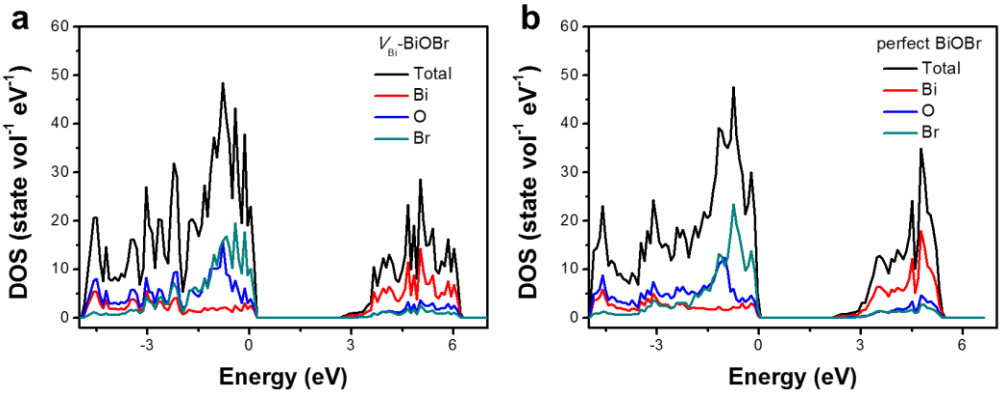


**Figure S8**. Calculated density of states of (a) $V_{Bi}$-BiOBr UNs and (b) perfect BiOBr with contribution of different atoms.

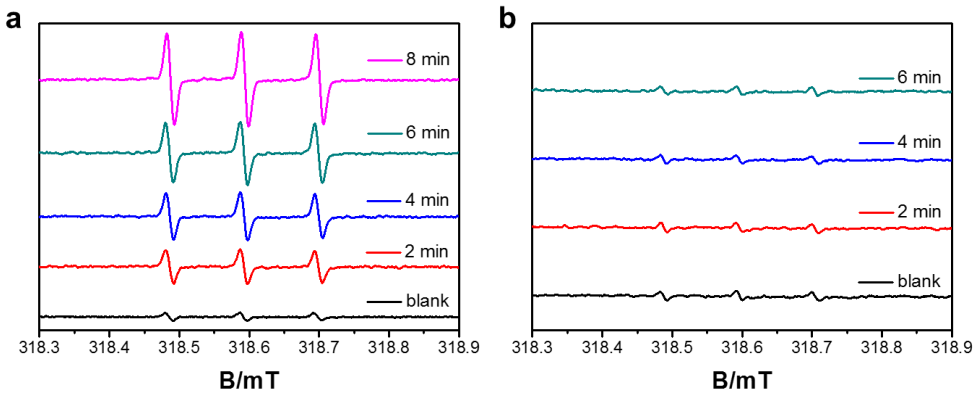


**Figure S9**. ESR spectra of (a) $V_{Bi}$-BiOBr UNs and (b) BiOBr nanosheets in the presence of 2,2,6,6-tetramethylpiperidine (TEMP) under irradiation.

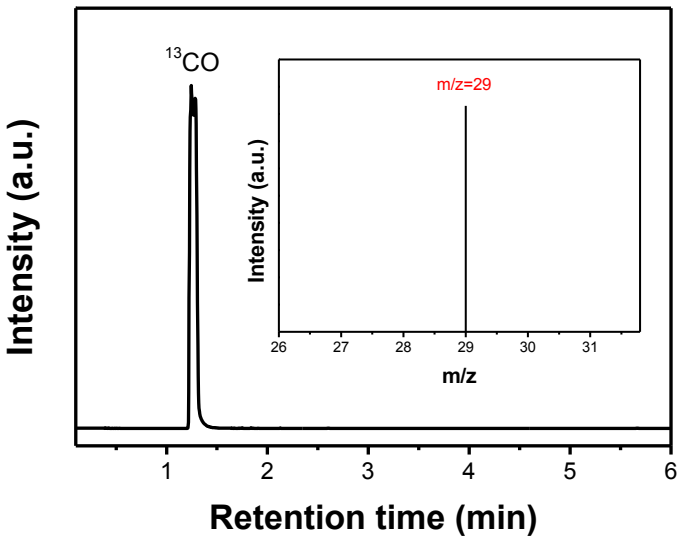


**Figure S10.** Mass spectra of $^{13}$CO (m/z = 29) produced over $V_{Bi}$-BiOBr UNs.

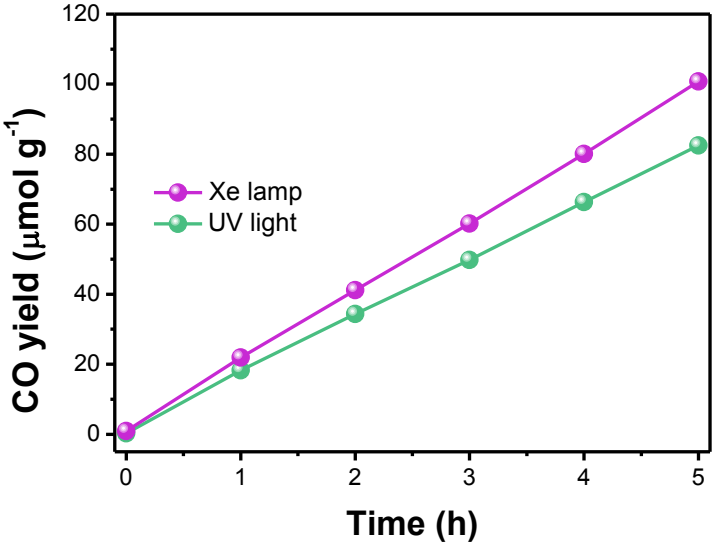


**Figure S11**. Photocatalytic CO evolution amount over $V_{Bi}$-BiOBr UNs under UV light irradiation.

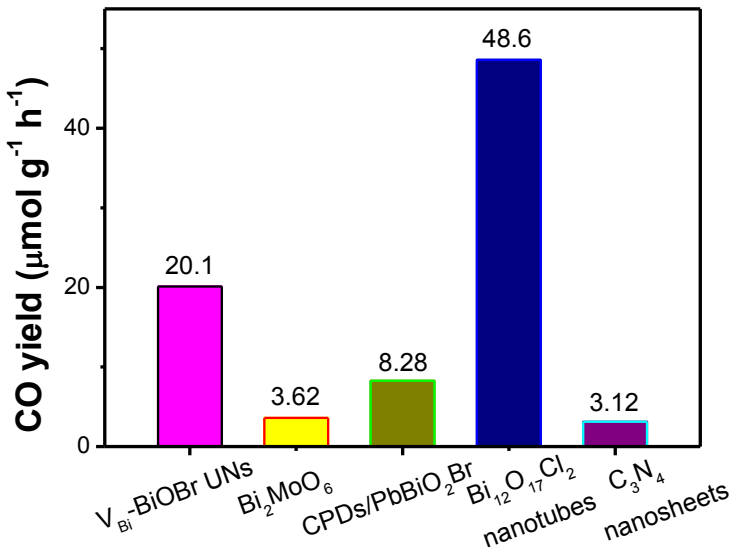


**Figure S12.** Performance comparison of several materials under the similar testing conditions.

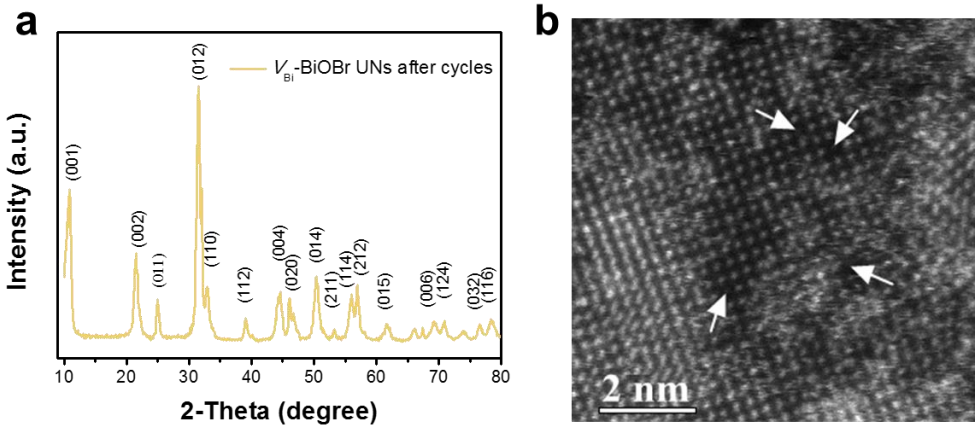


**Figure S13**. (a) XRD and (b) HAADF-STEM image of $V_{Bi}$-BiOBr UNs after cycles.

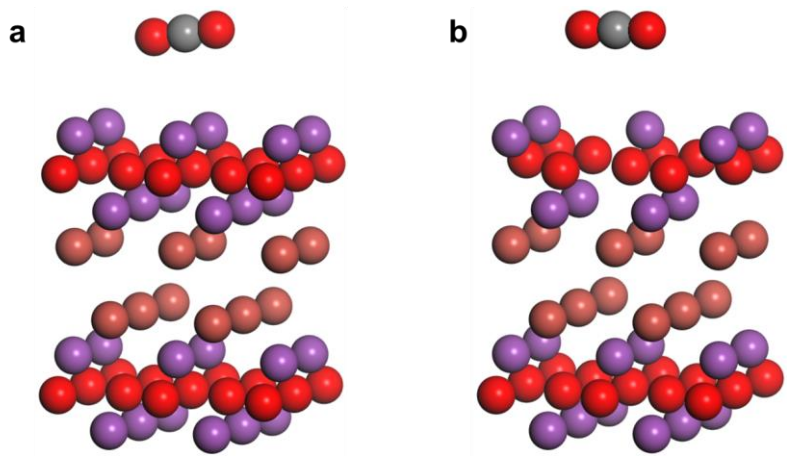


**Figure S14.** Schematic illustration of the adsorption of $CO_2$ molecules onto (a) perfect BiOBr and (b) $V_{Bi}$-BiOBr.

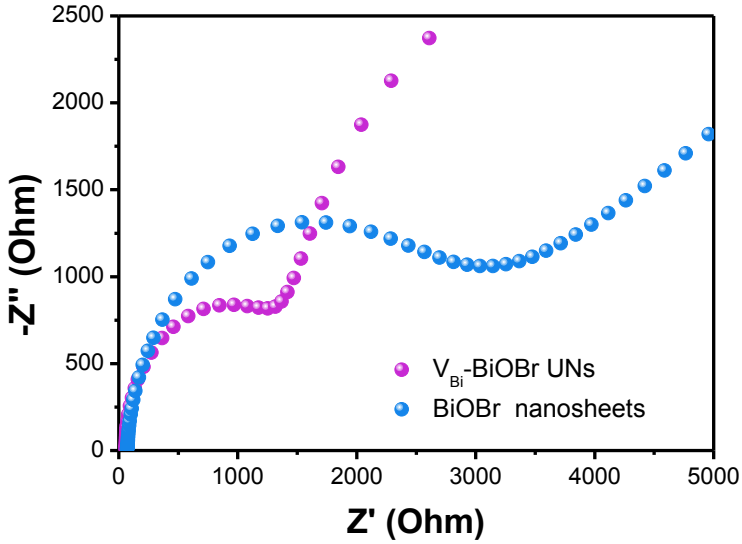


**Figure S15**. Electrochemical impedance spectra for $V_{Bi}$-BiOBr UNs and BiOBr nanosheets.

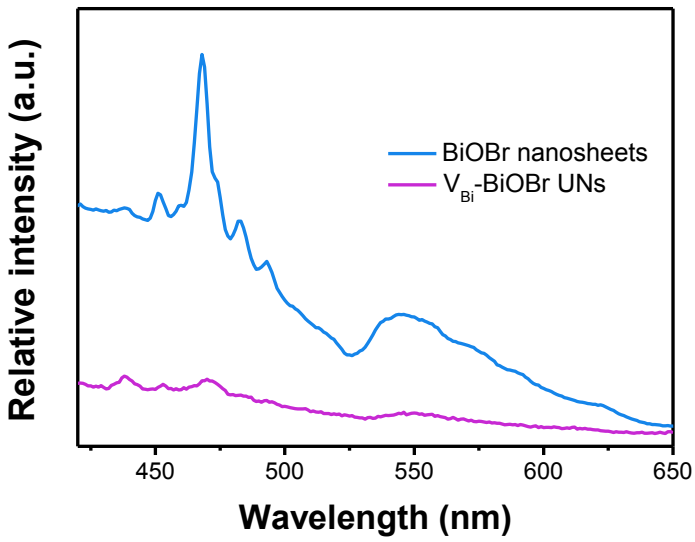


**Figure S16.** PL spectra of the $V_{Bi}$-BiOBr UNs and BiOBr nanosheets.

**Table S1**. Comparison of the reaction conditions and photocatalytic activity with other catalysts for $CO_2$ reduction to CO.

| **Photocatalysts** | **Light sources** | **Reaction conditions** | **Products** | **Photocatalytic efficiencies** | **Ref.** |
|---|---|---|---|---|---|
| $V_{Bi}$-BiOBr UNs | Xe lamp | Liquid-solid, water | CO | 20.1 μmol $g^{-1}$ $h^{-1}$ | This work |
| oxygen-rich $WO_3$ layers | IR light | Liquid-solid, water | CO | 2.8 μmol $g^{-1}$ $h^{-1}$ | S1 |
| BiOCl with oxygen vacancies | Xe lamp | Liquid-solid, water | CO | 1.01 μmol $g^{-1}$ $h^{-1}$ | S2 |
| monolayered BiOBr | Xe lamp | Gas-solid, water | CO | ~0.9 μmol $g^{-1}$ $h^{-1}$ | S3 |
| ultrathin ZnAl LDH | Xe lamp | Gas-solid, water | CO | 7.6 μmol $g^{-1}$ $h^{-1}$ | S4 |
| partially oxidized $SnS_2$ atomic layers | Visible light | Gas-solid, water | CO | 12.28 μmol $g^{-1}$ $h^{-1}$ | S5 |
| Co tuned Au nanoclusters | Visible light | Liquid-solid, water/ TEOA | CO | 3.45 μmol $g^{-1}$ $h^{-1}$ | S6 |
| Ni doped CdS quantum dots | Visible light | Liquid-solid, water/ TEOA | CO | ~9.5 μmol $g^{-1}$ $h^{-1}$ | S7 |
| g-$C_3N_4$@T-paper | Visible light | Gas-solid, water | CO | 0.16 μmol $g^{-1}$ $h^{-1}$ | S8 |
| carbon nitride nanosheets | Visible light | Liquid-solid, MeCN/TEOA = 4:1 | CO | 2.9 μmol $g^{-1}$ $h^{-1}$ | S9 |
| (001) facet exposed BiOBr | Xe lamp | Gas-solid, water | CO | 4.45 μmol $g^{-1}$ $h^{-1}$ | S10 |
| $Bi_4O_5Br_2$ | Visible light | Gas-solid, water | CO | 2.73 μmol $g^{-1}$ $h^{-1}$ | S11 |
| defective $Bi_2MoO_6$ | Xe lamp | Liquid-solid, water | CO | 3.62 μmol $g^{-1}$ $h^{-1}$ | S12 |
| $BiOIO_3$ {010}/{100} facet junctions | Xe lamp | Gas-solid, water | CO | 5.42 μmol $g^{-1}$ $h^{-1}$ | S13 |

| | | | | | |
|---|---|---|---|---|---|
| copper oxide nanoclusters-grafted $Nb_3O_8^-$ nanosheets | UV light | Liquid-solid, 0.5 M $KHCO_3$ aqueous solution | CO | ~0.68 μmol $g^{-1}$ $h^{-1}$ | S14 |
| Au-CNS-ZIF-9 | Xe lamp | Gas-solid, water | CO | ~0.5 μmol $g^{-1}$ $h^{-1}$ | S15 |
| ZrPP-1-Co | Visible light | Liquid-solid, MeCN/TEOA = 4:1 | CO | ~14 μmol $g^{-1}$ $h^{-1}$ | S16 |


[S1] Liang, L.; Li, X. D.; Sun, Y. F.; Tan, Y. L.; Jiao, X. C.; Ju, H. X.; Qi, Z. M.; Zhu, J. F.; Xie, Y. Infrared Light-Driven $CO_2$ Overall Splitting at Room Temperature. *Joule* **2018**, *2*, 1-13.

[S2] Zhang, L.; Wang, W. Z.; Jiang, D.; Gao, E. P.; Sun, S. M. Photoreduction of $CO_2$ on BiOCl Nanoplates with the Assistance of Photoinduced Oxygen Vacancies. *Nano Res.* **2015**, *8*, 821-831.

[S3] Yu, H. J.; Huang, H. W.; Xu, K.; Hao, W. C.; Guo, Y. X.; Wang, S. B.; Shen, X. L.; Pan, S. F.; Zhang, Y. H. Liquid-Phase Exfoliation into Monolayered BiOBr Nanosheets for Photocatalytic Oxidation and Reduction. *ACS Sustainable Chem. Eng.* **2017**, *5*, 10499-10508.

[S4] Zhao, Y. F.; Chen, G. B.; Bian, T.; Zhou, C.; Waterhouse, G. I. N.; Wu, L. Z.; Tung, C. H.; Smith, L. J.; O'Hare, D.; Zhang, T. R. Defect-Rich Ultrathin ZnAl-Layered Double Hydroxide Nanosheets for Efficient Photoreduction of $CO_2$ to CO with Water. *Adv. Mater.* **2015**, *27*, 7824-7831.

[S5] Jiao, X. C.; Li, X. D.; Jin, X. Y.; Sun, Y. F.; Xu, J. Q.; Liang, L.; Ju, H. X.; Zhu, J. F.; Pan, Y.; Yan, W. S.; Lin, Y.; Xie, Y. Partially Oxidized $SnS_2$ Atomic Layers Achieving Efficient Visible-Light-Driven $CO_2$ Reduction. *J. Am. Chem. Soc.* **2017**, *139*, 18044-18051.

[S6] Cui, X. F.; Wang, J.; Liu, B.; Ling, S.; Long, R.; Xiong, Y. J. Turning Au Nanoclusters Catalytically Active for Visible-Light-Driven $CO_2$ Reduction through Bridging Ligands. *J. Am. Chem. Soc.* **2018**, *140*, 16514-16520.

[S7] Wang, J.; Xia, T.; Wang, L.; Zheng, X. S.; Qi, Z. M.; Gao, C.; Zhu, J. F.; Li, Z. Q.;

Xu, H. X.; Xiong, Y. J. Enabling Visible-Light-Driven Selective $CO_2$ Reduction by Doping Quantum Dots: Trapping Electrons and Suppressing $H_2$ Evolution. *Angew. Chem. Int. Ed.* **2018**, *57*, 16447-16451.

[S8] Wang, Y. G.; Li, T.; Yao, Y. G.; Li, X.; Bai, X.; Yin, C. C.; Williams, N.; Kang, S. F.; Cui, L. F.; Hu, L. B. Dramatic Enhancement of $CO_2$ Photoreduction by Biodegradable Light-Management Paper. *Adv. Energy Mater.* **2018**, *8*, 1703136.

[S9] Shi, L.; Wang, T.; Zhang, H. B.; Chang, K.; Ye, J. H. Electrostatic Self-Assembly of Nanosized Carbon Nitride Nanosheet onto a Zirconium Metal-Organic Framework for Enhanced Photocatalytic $CO_2$ Reduction. *Adv. Funct. Mater.* **2015**, *25*, 5360-5367.

[S10] Wu, D.; Ye, L. Q.; Yip, H. Y.; Wong, P. K. Organic-Free Synthesis of {001} Facet Dominated BiOBr Nanosheets for Selective Photoreduction of $CO_2$ to CO. *Catal. Sci. Technol.* **2017**, *7*, 265-271.

[S11] Ye, L. Q.; Jin, X. L.; Liu, C.; Ding, C. H.; Xie, H. Q.; Chu, K. H.; Wong, P. K. Thickness-Ultrathin and Bismuth-Rich Strategies for BiOBr to Enhance Photoreduction of $CO_2$ into Solar Fuels. *Appl. Catal. B* **2016**, *187*, 281-290.

[S12] Di, J.; Zhao, X. X.; Lian, C.; Ji, M. X.; Xia, J. X.; Xiong, J.; Zhou, W.; Cao, X. Z.; She, Y. B.; Liu, H. L.; Loh, K. P.; Pennycook, S. J.; Li, H. M.; Liu, Z. Atomically-Thin $Bi_2MoO_6$ Nanosheets with Vacancy Pairs for Improved Photocatalytic $CO_2$ Reduction. *Nano Energy* **2019**, *61*, 54-59.

[S13] Chen, F.; Huang, H. W.; Ye, L. Q.; Zhang, T. R.; Zhang, Y. H.; Han, X. P.; Ma, T. Y. Thickness-Dependent Facet Junction Control of Layered $BiOIO_3$ Single Crystals for Highly Efficient $CO_2$ Photoreduction. *Adv. Funct. Mater.* **2018**, 1804284.

[S14] Yin, G.; Nishikawa, M.; Nosaka, Y.; Srinivasan, N.; Atarashi, D.; Sakai, E.; Miyauchi, M. Photocatalytic Carbon Dioxide Reduction by Copper Oxide Nanocluster-Grafted Niobate Nanosheets. *ACS Nano* **2015**, *9*, 2111-2119.

[S15] Zhou, H.; Li, P.; Liu, J.; Chen, Z. P.; Liu, L. Q.; Dontsova, D.; Yan, R. Y.; Fan, T. X.; Zhang, D.; Ye, J. H. Biomimetic Polymeric Semiconductor Based Hybrid Nanosystems for Artificial Photosynthesis towards Solar Fuels Generation via $CO_2$ Reduction. *Nano Energy* **2016**, *25*, 128-135.

[S16] Chen, E. X.; Qiu, M.; Zhang, Y. F.; Zhu, Y. S.; Liu, L. Y.; Sun, Y. Y.; Bu, X. H.;

Zhang, J.; Lin, Q. P. Acid and Base Resistant Zirconium Polyphenolate-Metalloporphyrin Scaffolds for Efficient $CO_2$ Photoreduction. *Adv. Mater.* **2018**, *30*, 1704388.